Images reveal that atmospheric particles can undergo liquid–liquid phase separations

Yuan You[a], Lindsay Renbaum-Wolff[a], Marc Carreras-Sospedra[b], Sarah J. Hanna[a], Naruki Hiranuma[c], Saeid Kamal[d], Mackenzie L. Smith[e], Xiaolu Zhang[f], Rodney J. Weber[f], John E. Shilling[g], Donald Dabdub[b], Scot T. Martin[e,h,1], and Allan K. Bertram[a,1]

[a]Department of Chemistry and [d]Laboratory for Advanced Spectroscopy and Image Research, University of British Columbia, Vancouver, BC, V6T 1Z1 Canada; [b]Department of Mechanical and Aerospace Engineering, University of California, Irvine, CA 92697; [c]Institute for Meteorology and Climate Research, Karlsruhe Institute of Technology, 76344 Eggenstein-Leopoldshafen, Germany; [g]Atmospheric Sciences and Global Change Division, Pacific Northwest National Laboratory, Richland, WA 99352; [e]School of Engineering and Applied Sciences and [h]Department of Earth and Planetary Sciences, Harvard University, Cambridge, MA 02138; and [f]School of Earth and Atmospheric Sciences, Georgia Institute of Technology, Atlanta, GA 30332

Edited by Mark H. Thiemens, University of California at San Diego, La Jolla, CA, and approved June 25, 2012 (received for review April 23, 2012)

A large fraction of submicron atmospheric aerosol particles contains both organic material and inorganic salts. As the relative humidity cycles in the atmosphere and the water content of the particles correspondingly changes, these mixed particles can undergo a range of phase transitions, possibly including liquid–liquid phase separation. If liquid–liquid phase separation occurs, the gas-particle partitioning of atmospheric semivolatile organic compounds, the scattering and absorption of solar radiation, and the reactive uptake of gas species on atmospheric particles may be affected, with important implications for climate predictions. The actual occurrence of liquid–liquid phase separation within individual atmospheric particles has been considered uncertain, in large part because of the absence of observations for real-world samples. Here, using optical and fluorescence microscopy, we present images that show the coexistence of two noncrystalline phases for real-world samples collected on multiple days in Atlanta, GA as well as for laboratory-generated samples under simulated atmospheric conditions. These results reveal that atmospheric particles can undergo liquid–liquid phase separations. To explore the implications of these findings, we carried out simulations of the Atlanta urban environment and found that liquid–liquid phase separation can result in increased concentrations of gas-phase NO_3 and N_2O_5 due to decreased particle uptake of N_2O_5.

chemistry | physical state | secondary organic aerosol | ambient aerosol | atmospheric chemistry

In the atmosphere, single particles containing both organic species and inorganic salts are abundant (1, 2). The number of different types of inorganic salts is relatively small, with ammonium sulfate considered to be one of the most important in particles less than 1 μm in diameter (3, 4). In contrast, the number of organic species in a single atmospheric particle is on the order of thousands, with only ~10% of these species identified at the molecular level (5). As the relative humidity (RH) cycles in the atmosphere through high and low values, the water content of the particles increases and decreases as a hygroscopic response. In response to variable water content, the mixed particles can undergo a range of phase transitions including crystallization (i.e., efflorescence), dissolution (i.e., deliquescence), and liquid–liquid phase separation (Fig. 1) (6–12).

Results of laboratory measurements or calculations for particles or solutions containing ammonium sulfate mixed with one or a few specific organic molecules suggest, after extrapolation to atmospheric conditions, that liquid–liquid phase separations can occur in atmospheric particles (6, 10, 13–16). Atmospheric particles, however, are far more complex than the simple proxies used in these studies. A few studies have inferred that liquid–liquid phase separation occurs in particles containing ammonium sulfate and secondary organic material (SOM) generated from the dark ozonolysis of α-pinene (17–20). In the present study, liquid–liquid phase separation is explored for real-world samples.

Results and Discussion

Up to 90% of the submicron particle-phase organic material in the atmosphere is SOM (5). In a first set of measurements focused on the laboratory samples, we investigated the phase behavior of particles consisting of ammonium sulfate mixed with SOM that had been produced for conditions designed to simulate natural and polluted atmospheres. For these experiments, α-pinene was ozonized, a process that is considered to be a major biogenic source of SOM in the atmosphere (5). As a surrogate of a polluted atmosphere, 1,2,4-trimethylbenzene was photooxidized (21). In both cases, the oxidation of the volatile organic compounds led to oxidized products having low vapor pressures, and these products condensed to form SOM. The SOM produced by these approaches contained tens to hundreds of oxygenated organic species (22) and, as such, can represent a good surrogate for oxygenated organic material widely prevalent in the atmosphere (5). The oxygen-to-carbon (O:C) elemental ratios of the SOM used in these experiments are listed in Table 1. These ratios fall within the range of values observed in the atmosphere (23).

The SOM was collected on filters, extracted with water, and combined with ammonium sulfate to prepare solutions having organic-to-sulfate (org:sulf) mass ratios of 1.4 and 3.0 for α-pinene and 1,2,4-trimethylbenzene, respectively. These org:sulf ratios were chosen to overlap with ratios often prevalent in the atmosphere (24, 25). The solutions were atomized onto Teflon slides, producing supermicron particles (10–30 μm in diameter). The Teflon slides were then placed in a flow cell having temperature and relative humidity control, and the microscopy experiments were carried out (13).

Shown in Fig. 2 are the optical and fluorescence images of the particles as a function of RH. Also included for comparison are images of pure ammonium sulfate particles. Included in *SI Text* are image movies of ammonium sulfate particles and ammonium sulfate–SOM particles recorded as the RH was decreased and increased (Movies S1, S2, S3, and S4).

Author contributions: Y.Y., L.R.-W., M.C.-S., S.J.H., N.H., S.K., M.L.S., X.Z., R.J.W., J.E.S., D.D., S.T.M., and A.K.B. designed research; Y.Y., L.R.-W., M.C.-S., S.J.H., N.H., S.K., M.L.S., X.Z., R.J.W., J.E.S., D.D., S.T.M., and A.K.B. performed research; Y.Y., L.R.-W., M.C.-S., S.J.H., N.H., S.K., M.L.S., X.Z., R.J.W., J.E.S., D.D., S.T.M., and A.K.B. analyzed data; and Y.Y., L.R.-W., M.C.-S., D.D., S.T.M., and A.K.B. wrote the paper.

The authors declare no conflict of interest.

This article is a PNAS Direct Submission.

[1] To whom correspondence may be addressed: E-mail: bertram@chem.ubc.ca or scot_martin@harvard.edu.

This article contains supporting information online at www.pnas.org/lookup/suppl/doi:10.1073/pnas.1206414109/-/DCSupplemental.

www.pnas.org/cgi/doi/10.1073/pnas.1206414109

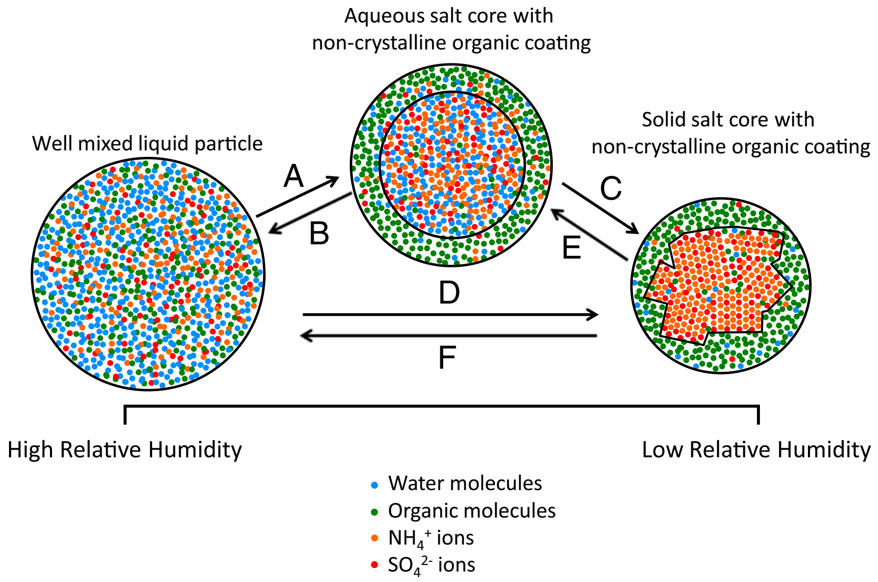

Fig. 1. Schematic of possible phase transitions of particles containing mixtures of oxygenated organic material and ammonium sulfate. Processes: (*A*) liquid–liquid phase separation, (*B*) liquid–liquid mixing, (*C* and *D*) inorganic efflorescence, and (*E* and *F*) inorganic deliquescence.

Particles of ammonium sulfate behaved as expected (Fig. 2 *A* and *B*). At 90%, 70%, and 50% RH the particles consisted of a single aqueous phase, and when the relative humidity was decreased from 90% to 50%, the particles decreased in size due to the loss of water. At 30% RH the particles were crystalline. In addition, the fluorescence signal was nearly negligible for the ammonium sulfate particles for all RH values. In comparison with these results for ammonium sulfate, images of particles consisting of SOM and ammonium sulfate (Fig. 2 *C*–*F*) indicated the presence of two distinct phases. In the optical images, the outer phase appeared as a dark perimeter ring. The phase separation was especially evident in the fluorescence images because of the contrast between the fluorescent outer phase and the nonfluorescent inner phase. The mixed particles of ammonium sulfate and SOM from the ozonolysis of α-pinene appeared to have two distinct phases, even at the upper end of the RH measurement at 90% RH (Fig. 2 *C* and *D*). The mixed particles of ammonium sulfate and SOM from the photooxidation of trimethylbenzene appeared to have two phases at RH values up to at least 70% (Fig. 2 *E* and *F*).

Several pieces of evidence indicate that the inner phase was inorganic rich and the outer phase was organic rich. First, the fluorescence signal, practically absent for pure ammonium sulfate particles, was confined mainly to the outer phase. Second, the inner phase crystallized at relative humidities between 35% and 40% RH (compare Movies S1, S2, S3, and S4). This range overlaps with the crystallization RH range of pure ammonium sulfate particles (∼33–37%) (26, 27). Third, the outer phase did not crystallize for the full range of RH values studied in our experiments, suggesting that there was negligible ammonium sulfate present in the outer phase. On the basis of these several observations, we conclude that the inner phase was an inorganic-rich phase and that the outer phase was an organic-rich phase. This conclusion is in agreement with previous Raman studies of particles containing ammonium sulfate and oxidized organic species (13, 14, 16).

We can also conclude from our results that both phases are noncrystalline above 35–40% RH. The presence of two separate noncrystalline phases confirms that liquid–liquid phase separation occurred in the particles, as molecular mobility is required for two phases to separate.

A few previous studies have inferred from laboratory studies that liquid–liquid phase separation occurs in particles containing ammonium sulfate and SOM generated from the dark ozonolysis of α-pinene (17–19). In these previous studies submicron particles were investigated. The consistency between the current results, which use supermicron particles, and these previous studies suggests that the liquid–liquid phase separations studied here do not depend strongly on particle size.

In the next set of measurements, we investigated the phase behavior of atmospheric samples collected in Atlanta, GA during

Table 1. Relevant information for samples

Particle type	O:C elemental ratio	Org:sulf mass ratio	NH_4^+ mass, mg	SO_4^{2-} mass, mg	NO_3^- mass, mg	Other inorganic ions mass*, mg	SRH, %
α-Pinene dark-ozonolysis SOM + $(NH_4)_2SO_4$	0.3	1.4	0.9	2.4	NA	NA	>90
1,2,4-trimethylbenzene photooxidation SOM + $(NH_4)_2SO_4$	0.4	3.0	2.3	6.2	NA	NA	>70
Atlanta organic sulfate July 28 and 29, 2010	0.5[†]	1.5	0.9	2.7	0.5	0.3	>90
Atlanta organic sulfate August 6 and 7, 2010	Unknown	1.0	2.0	4.7	0.9	0.2	>90

The table shows oxygen-to-carbon (O:C) elemental ratio of the organic material, organic-to-sulfate (org:sulf) mass ratio, mass of inorganic material, and the liquid–liquid separation relative humidities (SRH). NA, not applicable.

*Other inorganic ions: Na^+, K^+, Mg^{2+}, Ca^{2+}, and Cl^-.

[†] The O:C is based on a filter collected on July 29 and 30, 2010. We assume that the O:C was similar on July 28 and 29, because meteorological conditions and particle chemistry, such as org:sulf, concentrations of water-soluble organic carbon, and concentrations of inorganic ions did not change considerably over the 2 d.

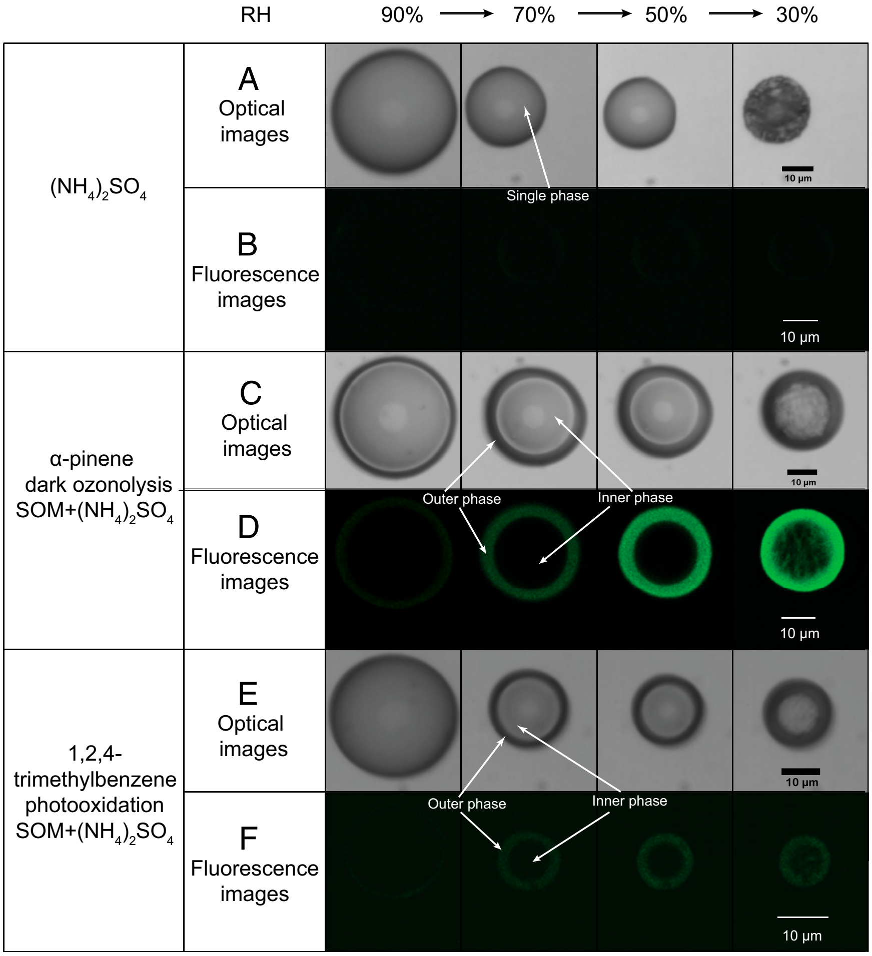

Fig. 2. Optical and fluorescence images of ammonium sulfate particles and ammonium sulfate–secondary organic material (SOM) particles at various relative humidities. Images were collected by optical reflectance microscopy and fluorescence microscopy for decreasing relative humidity. Rows: (*A* and *B*) optical and fluorescence images of a reference ammonium sulfate particle; (*C* and *D*) optical and fluorescence images of ammonium sulfate–SOM particle produced by α-pinene ozonolysis (org:sulf = 1.4); (*E* and *F*) optical and fluorescence images of ammonium sulfate–SOM particle produced by 1,2,4-trimethylbenzene photooxidation (org:sulf = 3). The light gray circle in the optical images at the center of all liquid droplets is an optical effect due to scattering by a spherical particle. This circle decreases in intensity or disappears after the inner phase crystallizes.

July and August 2010. The atmosphere in and around Atlanta is heavily influenced by both anthropogenic and biogenic emissions (28). Single-particle mass spectrometric measurements in Atlanta have shown that ambient particles typically occur as internal mixtures of organic molecules and sulfate (29, 30). For our study, atmospheric samples were collected on filters, and inorganic salts and water-soluble organic material were extracted with high-purity water. The resulting extract solutions were atomized onto Teflon slides, producing supermicron particles for the microscopy studies. The filter extracts were almost exclusively ammonium sulfate and organic material, with other species making up less than 10% of the total mass identified (see *Materials and Methods* and Table 1 for further details). Additional ammonium sulfate was not added to the Atlanta filter samples.

Shown in Fig. 3 are results from samples collected July 28 and 29 and August 6 and 7, 2010 in Atlanta. Included in the SI are movies for samples collected on August 6 and 7, 2010 in Atlanta, recorded as the RH was decreased and increased (Movies S5 and S6). The sequence of observations is qualitatively similar to that described for the laboratory-generated particles of mixed SOM and ammonium sulfate. Following a similar line of argument, we then conclude that the atmospheric samples from Atlanta also underwent liquid–liquid phase separation. A total of four samples collected on different days in Atlanta were analyzed, and in all cases results similar to those shown in Fig. 3 were observed.

As only the relatively water-soluble species were extracted from the filters, the experiments herein can be anticipated to be enriched in more-oxidized organic species in comparison to the atmospheric particles. However, less-oxidized species tend to favor liquid–liquid phase separation more strongly than do more-oxidized species (6, 13, 16). Therefore, our results showing that liquid–liquid phase separation occurs even for the more-oxidized fraction suggest that liquid–liquid phase separation will also occur for the whole composition, as present in ambient atmospheric particles.

Atmospheric Implications

Phase separation can influence the relative humidity at which crystallization and dissolution of sulfate solids occur in atmospheric particles (13, 14, 18) and thus can influence the extinction of solar radiation (31). Phase separation in atmospheric particles can also change the partitioning of organic molecules between the gas and particle phases. Thermodynamic calculations suggest that separation into organic-rich and inorganic-rich phases can increase the mass of organic material partitioning into the condensed phase by as much as 50% (6, 7).

Phase separation can also influence the reactive uptake of N_2O_5 into atmospheric particles (32–34). N_2O_5 is known to react

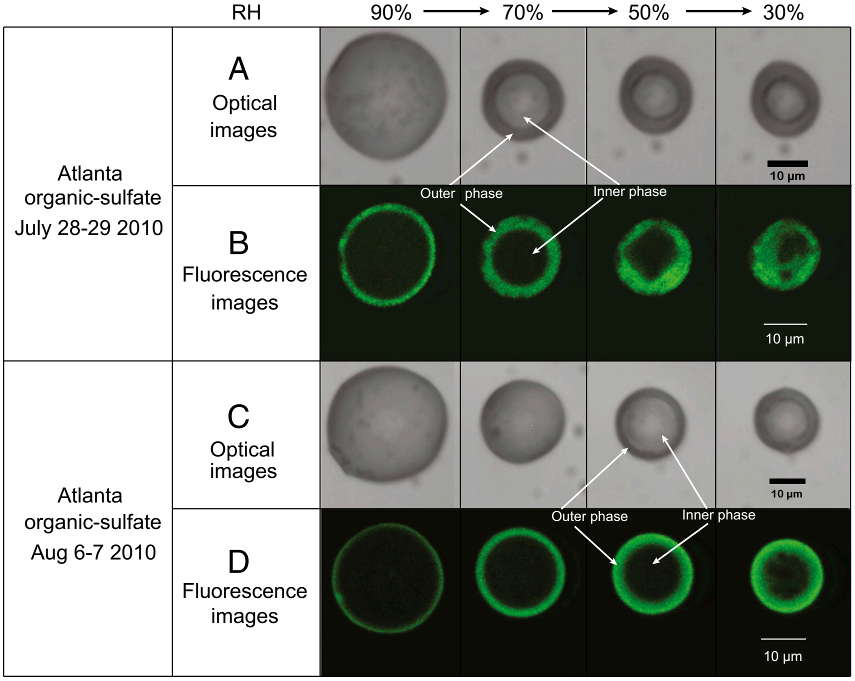

Fig. 3. Optical and fluorescence images of particles generated from filter samples collected in Atlanta, GA. Images were collected for decreasing relative humidity. From *Top* to *Bottom*: (*A* and *B*) optical and fluorescence images of a particle generated from a filter sample collected July 28 and 29, 2010; (*C* and *D*) optical and fluorescence images of a particle generated from a filter sample collected August 6 and 7, 2010.

efficiently on aqueous inorganic particles. Laboratory experiments show a significant decrease in N_2O_5 uptake for aqueous ammonium bisulfate particles coated with SOM (32, 33, 35). In addition, Reimer et al. (34) present simulations for Europe showing that liquid–liquid phase separation can effectively suppress N_2O_5 uptake onto particles in the atmosphere, leading to changes in mixing ratios of N_2O_5, NO_3, particle phase nitrate, and volatile organic compounds. A decrease in particle nitrate concentrations by up to 90% was simulated. Possibly related, Brown et al. show an anticorrelation between N_2O_5 reactive uptake and the organic-to-sulfate mass ratio for the northeastern United States (36).

To extend the simulations introduced by Reimer et al. but for the Atlanta environment, we used a box model to investigate the implications of liquid–liquid phase separation. Two different simulations were carried out. In case *a*, for N_2O_5 reactivity a homogeneous particle was assumed, and the rate of reaction depended only on the ratio of sulfate and nitrate in the particle (34, 37). In case *b*, for N_2O_5 reactivity an organic-rich coating and inorganic-rich core were assumed, and the rate of reaction depended both on the ratio of sulfate and nitrate in the core and the solubility and diffusion of N_2O_5 in the organic coating (34). The method of describing N_2O_5 reactive uptake followed that of Reimer et al. However, the model formulations used to describe the organic and inorganic particle concentrations as well as to treat liquid–liquid phase separation were different (*SI Text* and Table S1).

Fig. 4 shows the simulation results. The effect of the organic coating is evident in the N_2O_5 concentrations at nighttime and early morning (Fig. 4*B*). The organic coating reduces the uptake of N_2O_5 by particles. There is a resultant increase in gas-phase N_2O_5 and NO_3 concentrations by up to 15%. There is also a moderate reduction of gas-phase ozone concentrations (1% of ~30–50 parts per billion) in the morning (Fig. 4*C*), as explained by ozone titration with NO_x (NO_x = NO + NO_2) under low-sunlight intensities. The box model studies, taken together with the prior study of Reimer et al. (34), illustrate that liquid–liquid phase separation can impact concentrations of important atmospheric species.

For case *b* above we assume, similar to previous work, that the organic-rich phase will form a complete coating on the inorganic-rich core. This assumption is consistent with recent laboratory experiments that have shown a significant decrease in N_2O_5 uptake for aqueous ammonium bisulfate particles coated with SOM (32, 33, 35). A caveat, however, is that recent experiments using supermicron levitated particles illustrate that a partially engulfed structure can occur for mixed particles composed of aqueous salt solutions and organic molecules of low O:C values (11, 38, 39). Atmospheric particles that form an engulfed structure rather than a core-shell structure might have a considerably higher N_2O_5 uptake. Additional studies focusing on the factors influencing morphology after liquid–liquid phase separation would be beneficial to help resolve this issue.

The work reported here shows that liquid–liquid phase separation can occur in the atmosphere when the O:C ratio of the organic material is roughly ≤ 0.5. Additional studies are needed to determine whether these phase transitions also occur in the atmosphere when the O:C ratio is >0.5.

Materials and Methods

Production of Secondary Organic Material. Dark ozonolysis of α-pinene was performed in the Harvard Environmental Chamber to produce secondary organic material that then condensed on dry ammonium sulfate seed particles. Ammonium sulfate seed particles were introduced into the chamber by atomization of a solution of $(NH_4)_2SO_4$, which was then dried using a diffusion dryer. The α-pinene and ozone were introduced to the chamber by a flow of purified air. The setup and experimental conditions of the dark ozonolysis experiments were similar to those used by Shilling et al. (40). Flow into the continuous-flow chamber was fixed at 20 standard liters per minute (sLpm) during operation. The temperature and relative humidity inside the chamber were maintained at 25 °C and 40%, respectively. An Aerodyne high-resolution time-of-flight Aerosol Mass Spectrometer (HR-ToF-AMS) was used to determine the composition of the particles. The secondary organic material with ammonium sulfate seeds was collected at the outlet of the continuous-flow chamber onto

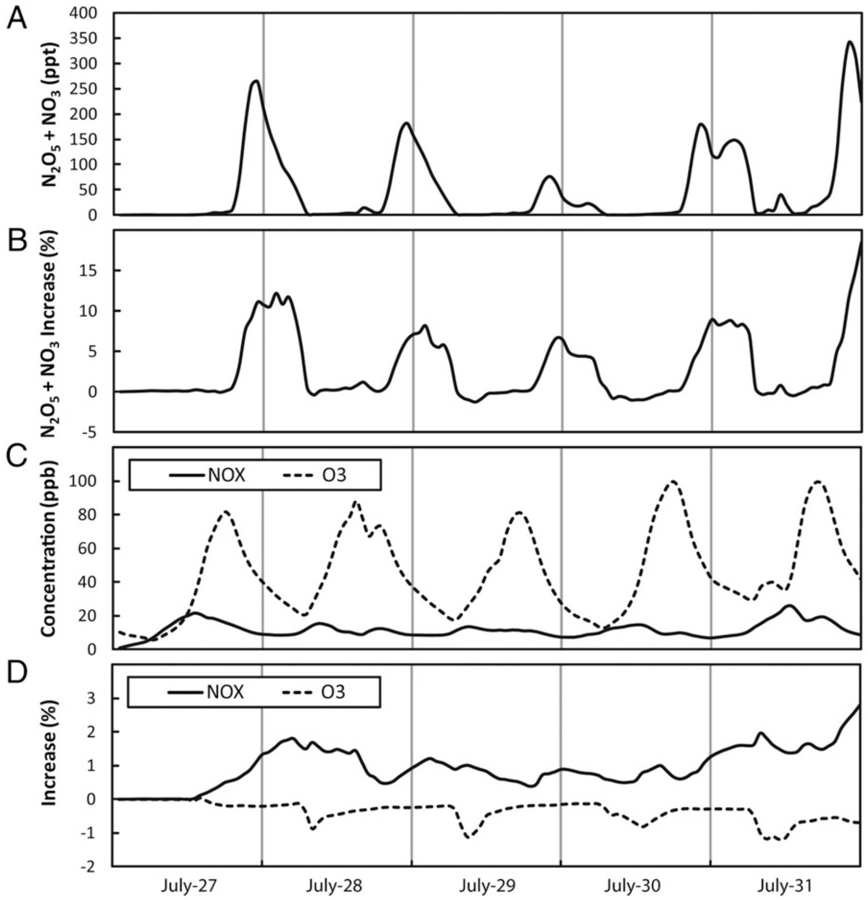

Fig. 4. Box model simulations for Atlanta, GA using meteorological conditions for the period July 27–August 1, 2010. (*A*) Modeled concentrations of N_2O_5 + NO_3 without the effect of organic coating. (*B*) Relative increase in N_2O_5 + NO_3 concentrations due to organic coatings. (*C*) Modeled absolute concentrations of NO_x and O_3 without the effect of organic coatings. (*D*) Relative increase in NO_x and O_3 concentrations due to organic coatings.

a quartz fiber filter. The collection time for sampling was 48 h at a flow rate of 9.0 sLpm.

Photooxidation of 1,2,4-trimethylbenzene was carried out in the Pacific Northwest National Laboratory (PNNL) Continuous-Flow Environmental Chamber to produce secondary organic material; 1,2,4-trimethylbenzene was injected into 24 sLpm of pure airflow to produce concentrations of 4.8 ppmv (parts-per-million by volume) in the chamber before reaction. An additional 1-sLpm flow of pure air was bubbled through a 50% (vol/vol) solution of hydrogen peroxide in water and added to the chamber. Photooxidation was initiated by 105 UV (Q-Laboratories UVA-340) lights surrounding the chamber, which generated OH radicals from the photolysis of hydrogen peroxide. The chamber temperature and relative humidity were maintained at 18.1 ± 0.2 °C and 6 ± 2%, respectively, over the course of the 4-d experimental run. NO_x levels were below the 1-ppbv (parts-per-billion by volume) detection limit of a NO_x chemiluminescence detector. Particle chemical composition was analyzed in real time, using an Aerodyne HR-ToF-AMS. The secondary organic material was collected at the outlet of the continuous-flow chamber onto a Teflon filter (Pall; R2PL037). The collection time for sampling was 82 h at a flow rate of 4 sLpm.

Collection of Samples from Atlanta, GA. Particles were collected on quartz fiber filters for ∼24 h, using a high-volume sampler (Thermo Anderson; flow rate 1.13×10^3 sLpm). Collection occurred on the Georgia Institute of Technology Environmental Science and Technology rooftop laboratory located in central Atlanta, ∼15 m above ground level. The concentration of organic carbon and inorganic salts on the filters was determined from 2.54-cm diameter filter punches, using a total organic carbon analyzer and ion chromatography. For the sample collected on July 28 and 29, 2010, the mass composition was the following: organic carbon = 3.99 mg; NH_4^+ = 0.859 mg, SO_4^{2-} = 2.711 mg, NO_3^- = 0.471 mg, Na^+ = 0.097 mg, K^+ = 0.043 mg, Mg^{2+} = 0.019 mg, Ca^{2+} = 0.068 mg, and Cl^- = 0.066 mg. For the sample collected on August 6 and 7, 2010, the composition was the following: organic carbon = 4.58 mg, NH_4^+ = 1.974 mg, SO_4^{2-} = 4.677 mg, NO_3^- = 0.902 mg, Na^+ = 0.074 mg, K^+ = 0.012 mg, Mg^{2+} = 0.012 mg, Ca^{2+} = 0.043 mg, and Cl^- = 0.049 mg. The O:C elemental ratio of the organic component of the filters collected in Atlanta was determined by extracting the filters with water and then determining the O:C from the filter extracts, using HR-ToF-AMS (41, 42).

Production of Particles. Water-soluble species were extracted from the filter samples, using Millipore water (18.2 MΩ cm). For the samples collected in Atlanta, particles were generated directly from the filter extracts without the addition of ammonium sulfate. Filter extracts were passed through a Particle-on-Demand Generator (model MJ-ABL-01–120; MicroFab Technologies) to produce particles with sizes ranging from 10 to 30 μm in diameter. These particles were deposited on Teflon slides and then placed in a flow cell that had temperature and relative humidity control for the microscopy experiments (43).

To increase the sulfate-to-organic mass ratio to values prevalent in the atmosphere (24, 25), ammonium sulfate solution was added to the filter extracts from the environmental chambers. After addition of ammonium sulfate, the organic-to-sulfate mass ratio in the samples from α-pinene and 1,2,4-trimethylbenzene were 1.4 and 3.0, respectively. Once ammonium sulfate was added to these filter extracts, they were used to produce particles as described above.

Optical and Fluorescence Microscopy of Particles. Images of the particles were recorded with fluorescence microscopy (Zeiss LSM510; $\lambda_{excitation}$ = 543 nm, $\lambda_{emission}$ = 650–710 nm, 293 ± 1 K) and optical light-reflectance microscopy (Zeiss Axiotech; 50× objective, 273 ± 1 K). At the beginning of an experiment, the RH in the flow cell was set to 90–100%, and the particles were allowed to equilibrate with the flow-cell RH for 15–20 min. The RH was then decreased at a constant rate (0.6%/min) while images were collected. Calibration of the absolute RH readings was performed using the deliquescence relative humidity values for pure ammonium sulfate particles. Ammonium sulfate particles were studied for comparison with the experimental samples. First a mixture of ammonium sulfate and high-purity water was prepared. This solution was then added to a blank filter and processed the same way as the filter samples discussed above.

Box Model Simulations. A box model was used to simulate chemistry in the Atlanta atmosphere. The size of the modeling region was set to 36 × 36 km (1,296 km^2) with a 600-m boundary layer height. Further details on the box model are given in *SI Text* and Table S1.

ACKNOWLEDGMENTS. This research was supported by the National Sciences and Engineering Research Council of Canada; US National Science Foundation Grants 0925467, 0802237, and 0909227; the Office of Science (BER) of the US Department of Energy; and the Pacific Northwest National Laboratory Aerosol Climate Initiative.

1. Murphy DM, et al. (2006) Single-particle mass spectrometry of tropospheric aerosol particles. *J Geophys Res* 111:D23S32.
2. Pratt KA, Prather KA (2010) Aircraft measurements of vertical profiles of aerosol mixing states. *J Geophys Res Atmos* 115:D11305.
3. Seinfeld JH, Pandis SN (2006) *Atmospheric Chemistry and Physics* (Wiley Interscience, Hoboken, NJ).
4. Finlayson-Pitts BJ, Pitts JN (2000) *Chemistry of the Upper and Lower Atmosphere: Theory, Experiments and Applications* (Academic, San Diego, London).
5. Hallquist M, et al. (2009) The formation, properties and impact of secondary organic aerosol: Current and emerging issues. *Atmos Chem Phys* 9:5155–5236.
6. Zuend A, Marcolli C, Peter T, Seinfeld JH (2010) Computation of liquid-liquid equilibria and phase stabilities: Implications for RH-dependent gas/particle partitioning of organic-inorganic aerosols. *Atmos Chem Phys* 10:7795–7820.
7. Chang EI, Pankow JF (2006) Prediction of activity coefficients in liquid aerosol particles containing organic compounds, dissolved inorganic salts, and water - Part 2: Consideration of phase separation effects by an X-UNIFAC model. *Atmos Environ* 40:6422–6436.
8. Martin ST (2000) Phase transitions of aqueous atmospheric particles. *Chem Rev* 100: 3403–3454.
9. Pankow JF (2003) Gas/particle partitioning of neutral and ionizing compounds to single and multi-phase aerosol particles. 1. Unified modeling framework. *Atmos Environ* 37:3323–3333.
10. Marcolli C, Krieger UK (2006) Phase changes during hygroscopic cycles of mixed organic/inorganic model systems of tropospheric aerosols. *J Phys Chem A* 110:1881–1893.
11. Buajarern J, Mitchem L, Reid JP (2007) Characterizing multiphase organic/inorganic/aqueous aerosol droplets. *J Phys Chem A* 111:9054–9061.
12. Clegg SL, Seinfeld JH, Brimblecombe P (2001) Thermodynamic modelling of aqueous aerosols containing electrolytes and dissolved organic compounds. *J Aerosol Sci* 32: 713–738.
13. Bertram AK, et al. (2011) Predicting the relative humidities of liquid-liquid phase separation, efflorescence, and deliquescence of mixed particles of ammonium sulfate, organic material, and water using the organic-to-sulfate mass ratio of the particle and the oxygen-to-carbon elemental ratio of the organic component. *Atmos Chem Phys* 11:10995–11006.
14. Ciobanu VG, Marcolli C, Krieger UK, Weers U, Peter T (2009) Liquid-liquid phase separation in mixed organic/inorganic aerosol particles. *J Phys Chem A* 113:10966–10978.
15. Erdakos GB, Asher WE, Seinfeld JH, Pankow JF (2006) Prediction of activity coefficients in liquid aerosol particles containing organic compounds, dissolved inorganic salts, and water - Part 1: Organic compounds and water by consideration of short- and long-range effects using X-UNIFAC.1. *Atmos Environ* 40:6410–6421.
16. Song M, et al. (2012) Liquid-liquid phase separation and morphology of internally mixed dicarboxylic acids/ammonium sulfate/water particles. *Atmos Chem Phys* 12: 2691–2712.
17. Anttila T, Kiendler-Scharr A, Mentel TF, Tillmann R (2007) Size dependent partitioning of organic material: Evidence for the formation of organic coatings on aqueous aerosols. *J Atmos Chem* 57:215–237.
18. Smith ML, Kuwata M, Martin ST (2011) Secondary organic material produced by the dark ozonolysis of alpha-pinene minimally affects the deliquescence and efflorescence of ammonium sulfate. *Aerosol Sci Technol* 45:225–242.
19. Prisle NL, Engelhart GJ, Bilde M, Donahue NM (2010) Humidity influence on gas-particle phase partitioning of alpha-pinene + O(3) secondary organic aerosol. *Geophys Res Lett* 37:L01802.
20. Zuend A, Seinfeld JH (2012) Modeling the gas-particle partitioning of secondary organic aerosol: The importance of liquid-liquid phase separation. *Atmos Chem Phys Discuss* 12:2199–2258.
21. Odum JR, Jungkamp TP, Griffin RJ, Flagan RC, Seinfeld JH (1997) The atmospheric aerosol-forming potential of whole gasoline vapor. *Science* 276:96–99.
22. Reinhardt A, et al. (2007) Ultrahigh mass resolution and accurate mass measurements as a tool to characterize oligomers in secondary organic aerosols. *Anal Chem* 79: 4074–4082.
23. Ng NL, et al. (2010) Organic aerosol components observed in Northern Hemispheric datasets from Aerosol Mass Spectrometry. *Atmos Chem Phys* 10:4625–4641.
24. Jimenez JL, et al. (2009) Evolution of organic aerosols in the atmosphere. *Science* 326: 1525–1529.
25. Zhang Q, et al. (2007) Ubiquity and dominance of oxygenated species in organic aerosols in anthropogenically-influenced Northern Hemisphere midlatitudes. *Geophys Res Lett* 34:L13801.
26. Pant A, Parsons MT, Bertram AK (2006) Crystallization of aqueous ammonium sulfate particles internally mixed with soot and kaolinite: Crystallization relative humidities and nucleation rates. *J Phys Chem A* 110:8701–8709.
27. Bodsworth A, Zobrist B, Bertram AK (2010) Inhibition of efflorescence in mixed organic-inorganic particles at temperatures less than 250 K. *Phys Chem Chem Phys* 12: 12259–12266.
28. Weber RJ, et al. (2007) A study of secondary organic aerosol formation in the anthropogenic-influenced southeastern United States. *J Geophys Res Atmos* 112: D13302.
29. Lee SH, Murphy DM, Thomson DS, Middlebrook AM (2002) Chemical components of single particles measured with Particle Analysis by Laser Mass Spectrometry (PALMS) during the Atlanta SuperSite Project: Focus on organic/sulfate, lead, soot, and mineral particles. *J Geophys Res Atmos* 107(D1):4003.
30. Liu DY, Wenzel RJ, Prather KA (2003) Aerosol time-of-flight mass spectrometry during the Atlanta Supersite Experiment: 1. Measurements. *J Geophys Res Atmos* 108:8426.
31. Martin ST, et al. (2004) Effects of the physical state of tropospheric ammonium-sulfate-nitrate particles on global aerosol direct radiative forcing. *Atmos Chem Phys* 4(1):183–214.
32. Anttila T, Kiendler-Scharr A, Tillmann R, Mentel TF (2006) On the reactive uptake of gaseous compounds by organic-coated aqueous aerosols: Theoretical analysis and application to the heterogeneous hydrolysis of N2O5. *J Phys Chem A* 110: 10435–10443.
33. Folkers M, Mentel TF, Wahner A (2003) Influence of an organic coating on the reactivity of aqueous aerosols probed by the heterogeneous hydrolysis of N2O5. *Geophys Res Lett* 30:1644.
34. Riemer N, et al. (2009) Relative importance of organic coatings for the heterogeneous hydrolysis of N2O5 during summer in Europe. *J Geophys Res Atmos* 114: D17307.
35. Escorcia EN, Sjostedt SJ, Abbatt JPD (2010) Kinetics of N(2)O(5) hydrolysis on secondary organic aerosol and mixed ammonium bisulfate-secondary organic aerosol particles. *J Phys Chem A* 114:13113–13121.
36. Brown SS, et al. (2006) Variability in nocturnal nitrogen oxide processing and its role in regional air quality. *Science* 311:67–70.
37. Riemer N, et al. (2003) Impact of the heterogeneous hydrolysis of N2O5 on chemistry and nitrate aerosol formation in the lower troposphere under photosmog conditions. *J Geophys Res Atmos* 108:4144.
38. Kwamena NOA, Buajarern J, Reid JP (2010) Equilibrium morphology of mixed organic/inorganic/aqueous aerosol droplets: Investigating the effect of relative humidity and surfactants. *J Phys Chem A* 114:5787–5795.
39. Reid JP, et al. (2011) The morphology of aerosol particles consisting of hydrophobic and hydrophilic phases: Hydrocarbons, alcohols and fatty acids as the hydrophobic component. *Phys Chem Chem Phys* 13:15559–15572.
40. Shilling JE, et al. (2008) Particle mass yield in secondary organic aerosol formed by the dark ozonolysis of alpha-pinene. *Atmos Chem Phys* 8:2073–2088.
41. Aiken AC, et al. (2008) O/C and OM/OC ratios of primary, secondary, and ambient organic aerosols with high-resolution time-of-flight aerosol mass spectrometry. *Environ Sci Technol* 42:4478–4485.
42. DeCarlo PF, et al. (2006) Field-deployable, high-resolution, time-of-flight aerosol mass spectrometer. *Anal Chem* 78:8281–8289.
43. Parsons MT, Mak J, Lipetz SR, Bertram AK (2004) Deliquescence of malonic, succinic, glutaric, and adipic acid particles. *J Geophys Res* 109:D06212.